Fundamental Principles and Issues of High-speed Piezoactuated Three-legged Motion for Miniature Robots Designed for Nanometer-scale Operations

Sylvain Martel

The International Journal of Robotics Research 2005; 24; 575
DOI: 10.1177/0278364905055594

Sylvain Martel

NanoRobotics Laboratory
Department of Computer Engineering and
Institute of Biomedical Engineering
École Polytechnique de Montréal (EPM)
PO Box 6079, Station Centre-ville
Montréal (Québec) Canada H3C 3A7
sylvain.martel@polymtl.ca
www.nano.polymtl.ca

Fundamental Principles and Issues of High-speed Piezoactuated Three-legged Motion for Miniature Robots Designed for Nanometer-scale Operations

Abstract

One of the important aspects in the development of high-throughput platforms based on a fleet of scientific instruments in the form of miniature wireless robots designed for fast operations at the nanometer-scale, is the conception of an embedded locomotion system capable of fast displacements between two successive locations while being accurate enough to position the robot within the range of the embedded instrument, typically within a few tenths of nanometers. This paper describes not only the fundamental principles of the locomotion method and mechanisms but the main constraints, challenges, and environmental conditions that must be taken into account in the implementation of such a system. Preliminary experimental results show the validity of this approach.

KEY WORDS—nanorobotics, nanometer scale, locomotion, miniature robots, piezoelectric, piezoceramic

1. Introduction

Robots may take various forms, and ideally they must be well adapted for the environment and the tasks being targeted. This basic principle also holds true in one aspect of nanorobotics, which is related to the conception of robots especially designed to operate at the nanoscale. The idea of using a fleet of miniature instrumented mechatronic systems in the form of robots for operations at the nanoscale is relatively recent (Martel et al. 1999). Research in this field, although promising, is still in its infancy compared to previous efforts performed in the field of microrobotics (Fukada and Ueyama 1994; De Ambroggi, Fortuna, and Muscato 1997; Rembold and Fatikow 1997; Ferreira, Fontaine, and Minotti 2000; Juhas et al. 2000, 2001). This interaction at the nanoscale is typically achieved by embedding a high-speed scanning probe microscope (SPM) tip or probing system, such as a scanning tunneling microscope (STM) or an atomic force microscope (AFM).

Mechanochemical or mechanosynthesis (Drexler 1981; Farell and Levinson 1985; Merkle 1993), where mechanical means are used to assemble atoms and/or molecules to construct new molecular structures, is one obvious example where robots may play an important role as a complementary process to other techniques used in nanotechnology. Other possible applications in a much shorter term are those where SPMs are presently used; these include, but are not limited to, surface sciences and metrology where high-speed nanotopography of a surface is essential in cases where surface finish is crucial, the investigation of surface deposition, etc. In other applications, the high spatial resolution of an embedded instrument such as the STM may provide an important complement to other imaging systems, such as the scanning electron microscope (SEM).

It is expected that the standard robotic-based manufacturing model where the whole task is divided into many subtasks executed in a pipeline fashion will not yield the highest throughput for many applications at the nanoscale. This is particularly true when considering the complexity and

The International Journal of Robotics Research
Vol. 24, No. 7, July 2005, pp. 575-588,
DOI: 10.1177/0278364905055594

difficulty of completing many subtasks at such a scale. The lack of predicting the exact time required to execute a particular subtask may cause a major bottleneck in the pipeline and hence decrease substantially the overall throughput of the system.

The proposed model is very different from other micro/nanofactory approaches (Breguet, Schmitt, and Clavel 2000) including the use of an SEM as the main platform (Aoyama and Fuchiwaki 2001). Unlike other approaches, the aim of the proposed platform is to maximize the throughput of operations performed at the nanoscale. As such, the method relies on a platform (Martel et al. 2001b, 2001c, 2002; Martel and Hunter 2002, 2004) where a fleet of mesoscale ($\sim 32 \times 32 \times 30$ mm^3) autonomous wireless instrumented robots called NanoWalker robots (Martel et al. 1999, 2000a, 2000b, 2001a, 2001d), capable of nanometer-scale operations, are available to execute a given task. The system proposes a task-oriented approach where the general information about the task to be executed by the platform is communicated between a user and the central computer through a special graphical user interface (GUI) appropriate for the task. Then, the central computer assigns each associated subtask to a particular robot according to several factors such as the type of instrument embedded onto the robot, its availability, and its location. The level of miniaturization of each robot without affecting the performance of each unit is also a key concept here since it allows us to increase the density of robots per surface area, yielding an increase of the overall throughput of the platform. This higher density of robots also increases the possibility to have at any given time a robot available to continue a subtask completed by a previous robot armed with a different tool and may help to lower the average travel distance between successive working locations for each robot.

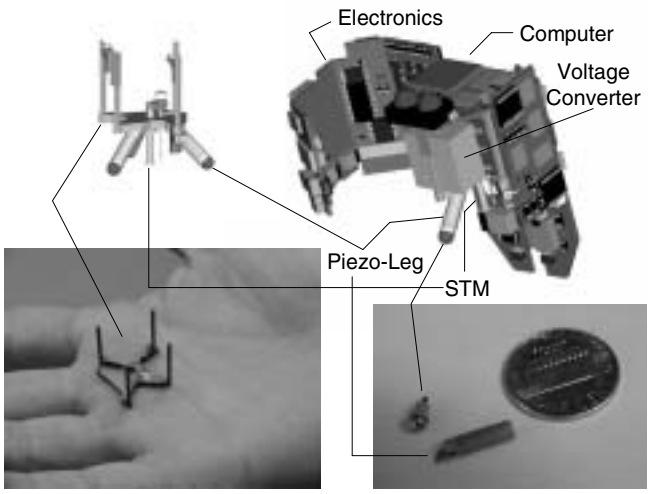

Fig. 1. Computer-aided design (CAD) representation showing the piezolegs as part of the NanoWalker robot (top) with a picture of the mechanical frames where the three legs are mounted in a pyramidal fashion (left) and the main components of a piezoleg beside a US penny (right).

2. Actuation System

The efficiency of the locomotion system embedded onto each robot is important in this particular context in order to minimize travel time. During travel, no useful work is being done at the nanoscale, which contributes to lowering the overall throughput of the platform. Hence, minimizing the time of travel is one of the critical aspects necessary to achieve the highest possible throughput for operations performed at the nanoscale. On the other hand, the locomotion system must allow for small step increments not greater than a few tenths of nanometers in order to position the robot within the scanning range of the embedded instrument. As such, locomotion methods for miniature robots at the nanoscale typically differ from the locomotion mechanisms that have been proposed at the mesoscale and microscale.

At the nanoscale, piezoceramic actuators have been intensively used in the recent years in high precision translation systems and in precise robotic applications. The small deflection amplitudes coped with the high resonant frequencies allow fast displacements with small step sizes required for accurate positioning. For instance, piezoceramic bimorph actuators have been used in the MINIMAN series of robots (Fahlbusch et al. 1999; Schmoeckel and Wörn 2001) using a stick-slip locomotion technique (Breguet, Pernette, and Clavel 1996).

In our actual implementation, each robot relies on three embedded piezoceramic actuators in a tubular form as depicted in Figure 1 to travel across the platform. The three piezotube actuators embedded onto each robot are mounted in a pyramidal fashion with the apex pointing upward, allowing faster locomotion speeds compared to previous methods.

2.1. Piezoceramic Legs

Piezoceramic actuators in tubular form are used to implement the legs of the robot. The tube consists of four external quadrant electrodes and an inner ground electrode. By applying voltage signals to the quadrant electrodes, bending and/or stretching in the form of contraction or extension of the piezotube can be achieved. Hence, bending in the X-axis and/or Y-axis, as depicted in Figure 2, and stretching along the Z-axis (longitudinal axis along the piezotube) offer the required flexibility for adequate motion.

Typically, to improve the overall linearity and to maximize the amplitude of deflection within the constraints of the embedded electronics, a symmetric-voltage mode is used. The symmetric-voltage mode consists of two voltage signals $(+V_y + V_z)$ and $(-V_y + V_z)$ equal in magnitude and opposite in sign that are applied to reciprocal electrodes on the

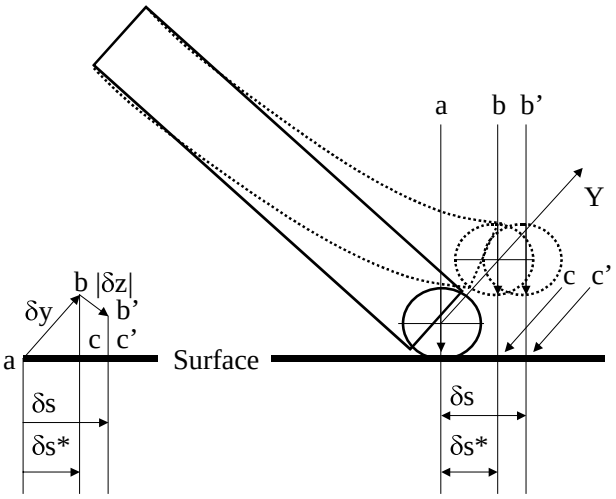

Fig. 2. Deflection and stretching of a piezoleg (not to scale).

piezoleg. Due to a corresponding electric field that is generated across the wall of the piezotube, a deflection of magnitude δy in the Y-axis for instance is obtained. The magnitude of such deflection can be computed as

$$\delta y = k \times V_{sy}, \tag{1}$$

$$V_{sy} = \frac{\left(+V_y + V_z\right) - \left(-V_y + V_z\right)}{2}. \tag{2}$$

In eq. (1), k is the piezoconstant and V_{sy} is the applied symmetric or bipolar voltage for the Y-axis (see Figure 2). In eq. (1), the piezoconstant is defined as

$$k = \frac{2\sqrt{2}d_{31}L^2}{\pi dh}. \tag{3}$$

In eq. (3), L is the length of the piezotube, d is the tube inner diameter, h is the wall thickness, and d_{31} is a standard piezoelectric coefficient. Angular deflections in the X–Y plane can also be achieved with proper voltage levels applied to the X- and Y-electrode pairs. Contraction or extension of the piezoleg is achieved by applying voltage levels with the same polarity to all four external electrodes simultaneously. This is referred here to as the stretching mode. The amplitude of contraction or extension of the piezotube in the stretching mode can be computed as

$$\delta z = \frac{-d_{31}L}{h} V_z. \tag{4}$$

The minus sign in front of the piezoconstant is arbitrary chosen such that a positive value will indicate that the leg termination or "foot" is moving upward toward the $+Z$-axis.

As depicted in Figure 2, deflection and stretching can be combined simultaneously. When such combination occurs, we refer to it here as the combined mode (Martel, Saraswat, and Hunter 2000c) for convenience. As depicted in Figure 2, the deflection of the leg in combined mode results in a horizontal projection vector denoted δs where $\delta s > \delta s^*$ for extension and $\delta s < \delta s^*$ for compression. Similarly, a smaller δs can be achieved in the combined mode (instead of using the bending mode only) if $\min\delta s^*$ is used with compression. On the other hand, the vector of the maximum horizontal projection, in the combined mode represented by the vector $a - c'$ in Figure 2, is typically smaller than the vector $a - c$ in Figure 2, being the maximum horizontal projection in the bending mode, i.e., $\max\delta s^* > \max\delta s$ under normal conditions.

2.2. Actuation Voltage Levels

Piezoactuators typically require relatively high voltage levels to operate and this is a major constraint in miniaturization. Most of the electronics embedded onto each miniature robot and particularly the digital electronics will operate at a relatively low voltage, typically of the order of +5 VDC and +3.3 VDC. Although some embedded analog electronics in the present implementation would need voltage levels up to ±15 VDC, the actuation voltage levels for the piezoactuators on the present implementation can reach maximum levels of ±150 VDC. Since most of the power of the embedded electronics requires relatively low supply voltage levels, two DC/DC converters are used to convert in our particular case the +5 VDC to ±150 VDC levels for actuation of the piezolegs.

As shown in eqs. (1) and (4), larger deflection and/or stretching amplitudes can be achieved with higher voltage levels. As the size of the robot decreases, the length of the piezoactuator decreases as well and according to eqs. (3) and (4), this will reduce the deflection and stretching amplitudes accordingly. Hence, a reduction of the length of the legs could be compensated with higher voltage levels. However, as shown in Figure 3 by the size of the DC/DC converters, voltage or power conversion takes most of the space in the actual implementation of the miniature robot and for a given energy that must be delivered to the piezoelectrodes in a very short time period; actual technologies make further miniaturization very difficult. Furthermore, ±150 VDC is presently the maximum practical voltage level that can be safely applied to these piezotubes (assuming piezoceramic such as PZT-5A) to avoid depolarization or loss of piezoeffects, and it is already too high if the legs are implemented with some other types of piezoceramic materials, such as PZT-5H for instance.

According to eqs. (3) and (4), besides the selection of a piezoceramic with higher value of d_{31}—such as the use of PZT-5H (if voltage levels in the implementation are limited to lower values) to increase the amplitude at the cost of added hysteresis, which is not a real concern for this type of

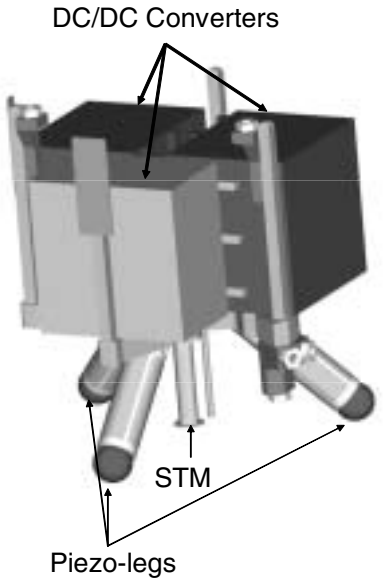

Fig. 3. CAD representation showing the space occupied by the voltage level converters with respect to the piezolegs.

locomotion—deflection and stretching amplitudes can also be increased by decreasing the wall thickness of the tube. This is possible but limited by the manufacturing process of the piezotube. Furthermore, since the piezolegs are supporting the whole structure of the robot, reducing the wall thickness may yield a structure too weak to support the weight of the robot.

It is also possible to increase the amplitude of deflection by using a bimorph piezoceramic structure or to implement a structure with mechanical amplification often used in other miniature robots. These approaches would unfortunately lower the force generated by the actuator, a factor not suitable in our case for reasons explained later.

2.3. Pyramidal Actuation Structure

The proposed actuation structure relies on three legs to minimize the size of the robot. Because of the additional drive electronics and the voltage conversion circuitries required for each leg, it is essential to minimize the number of piezolegs in order to achieve the highest level of miniaturization of the robot. Three legs, as depicted in Figure 3, provide the minimum number of contact points to guarantee static stability of the structure, a similar approach to the triangular of support in ants (Zollikofer 1994).

The drawback of such tripod structure is that it becomes unstable during the displacement of the robot as opposed to a four-legged structure that would maintain at least three contact points with the surface at any given time. This instability is managed in part by an onboard digital signal processing (DSP) system. The fact that microelectronics can be implemented in a very small form factor allows us to embed sufficient computation to control and correct sufficiently for such instability.

Piezoactuation systems for microrobots of this type typically rely on a stick–slip method of motion. During the stick phase, the force of the piezoleg does not exceed the static friction force and the structure of the robot is displaced due to the bending of the legs. This stick phase is followed by the slip phase, where the legs make an abrupt movement fast enough to not cause a large movement in the reverse direction. In this case, the coefficient of friction between the extremities of the legs or "feet" and the walking surface has to be low enough to allow the slip phase to occur. In this particular approach, the legs are typically mounted vertically or 90° from the walking surface. In such a configuration, the step size is determined by the amplitude of deflection of the piezolegs. To achieve faster displacement speeds, the new structure has the legs mounted as a pyramid at 45° from the floor with the apex pointing upward. Unlike the previous methods, the proposed method uses the static force of friction to build up an initial force and then creates a large acceleration of the legs. With a 45° angle, step sizes larger than the maximum amplitude of deflection of the piezolegs (see eq. (1) and the experimental results at the end of this paper) can be achieved, yielding faster displacement rates (especially in the directions A090°, B090°, and C090° because of the reciprocal pushing action of two reciprocal legs; see Figure 4) than can be achieved with the previous methods.

2.4. Control of Motion Vectors

For convenience, the three-legged configuration is represented by a special coordinate system (Martel, Saraswat, and Hunter 2000c), which is shown in Figure 4. With this representation, the direction of motion is always referred to one of the three legs. For instance, the direction denoted A090° indicates an angle of 90° counterclockwise from the X-axis of leg A (A-leg). For the push component in the push–slip walking method described later in this paper, the concept of a pressure zone is introduced. The pressure zone (as depicted in Figure 4) is defined as a region where a deflection using bending forces only of the corresponding leg will lead to an increase of the pressure between the leg and the walking surface on a frictionless surface. The pressure is maximum when a deflection is made toward the apex (center of the robot), i.e., with an angle of V(–135°). In practice, the stretching forces acting on the longitudinal direction of the leg can also be used to create pressure for pushing action during the push–slip motion, and such a region will expand from the apex under various coefficients of friction.

For convenience, leg A of the robot is the reference leg and coordinates on the horizontal plane based on such a reference can also be denoted H000° ≡ A000° to H359° ≡ A359°. As

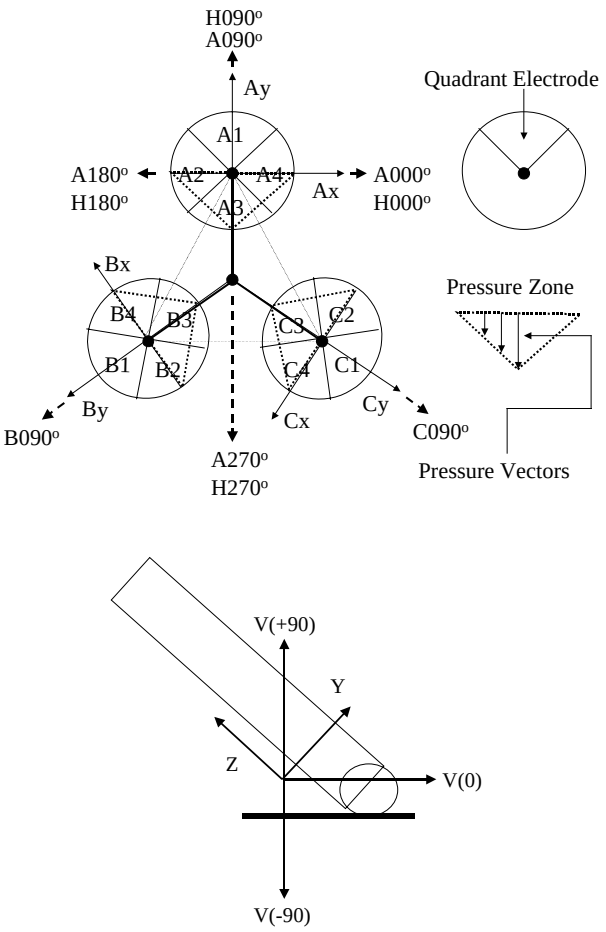

Fig. 4. Coordinate system for the three-legged locomotion architecture.

depicted in Figure 4, each leg has also its own X-, Y-, and Z-axis. For instance, the X-axis for leg A is denoted Ax. Vertical motions are also referred to as a vertical angle as depicted in Figure 4. When only vertical and horizontal directions are being referred to, the notations +H-axis, –H-axis, +V-axis, and –V-axis are also used for convenience here to represent V(0°), V(180°), V(+90°), and V(–90°), respectively.

For proper motion, a fundamental law for this configuration is to create resultant bending force vectors that are not directed toward any pressure zones while acting toward the direction of the desired motion. For example, if a motion in the H090° direction is required, leg A can be deflected toward A090° while legs B and C are deflected in a direction set between electrodes B1–B4 and C1–C2, respectively. This particular approach typically gives good results when the force of friction is very low, since initially the friction will act against the motion of the legs.

On the other hand, with an increase of the force of friction and/or a decrease of the maximum slew rate achievable by the onboard electronics (due to constraints imposed by the level of miniaturization), the force of friction acting against the legs can initially be used to provide a pushing action. When this pushing action is integrated onto the method of motion, we refer to it as a push–slip method. A strategy to compensate for an increase of the coefficient of friction between a robot and the surface is to rotate the resultant force vector from B2 and C4 (to compensate for the lack of friction) by increasing the pressure with the surface (in the direction of B090° and C090°, respectively) with sufficient level of friction. A small compression can also be used for the front leg (e.g., leg A) in order to minimize a force component reciprocal to the direction of motion. Similarly, the initial forces of friction acting against legs B and C would create a reciprocal pushing action on the back legs, allowing the robot to move toward the direction A090°.

Other approaches are also possible. For instance, a larger force of motion can also potentially be achieved by rotating the resultant force of motion of legs B and C toward H270° (approximately between electrodes B1–B2 and C1–C4, respectively). Motion in any directions (including clockwise and counterclockwise rotational motions), as demonstrated in the experimental results section of this paper, can be achieved with various combinations and directions of the force vectors.

We recall that a pushing action can be based on reciprocal friction forces and/or pressure forces as defined in this paper. Initially, if we consider the case where only the forces of friction are used to create the pushing forces, the generation of a bending force using B2 and B4 electrodes to push the robot toward A090° while maintaining B1 and B3 at 0 V, a bending horizontal component force $F_B \leq \max F_s$ can be created, as depicted in Figure 5. This bending force creates a reciprocal pushing force of the same magnitude and denoted F_{sB} that increases through the static phase up to a maximum amplitude designated $\max F_s$. If the static coefficient of friction is too small to cause an adequate motion, more pressure can be exerted using one of several possible approaches. One simple solution is to apply a small voltage level to the electrode pair B1–B3. This will cause a small deflection of the piezoleg toward B270° resulting in a small corrective force component F_c. This corrective force component causes the resulting bending force to shift anticlockwise to a new resultant force F_{Bc}. This is shown in Figure 5. In turn, this new resultant force creates an opposite pushing force $F_{sBc,}$ decreasing the amplitude of the pushing force on the A090° axis compared to F_{sB}. Another yet more efficient approach is to create an additional bending force toward B090°. This bending force can act in a manner such that a clockwise rotation of the resultant bending force can be observed. A bending force of the same magnitude as that used with the B2–B4 electrode pair would also likely generate a pushing force F_{st}. When combined with F_{sB}, it would provide the resulting pushing force F_{pB}, as shown in Figure 5. This pushing force is not directly oriented toward A090°, and hence F_{st} could be reduced to F'_{st} with a reduction

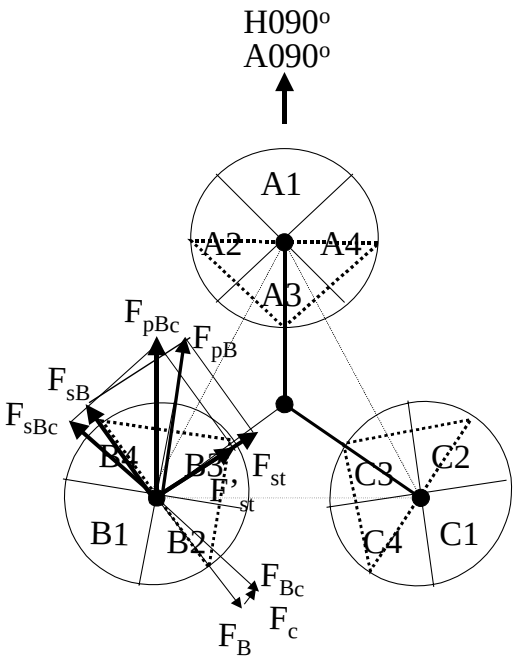

Fig. 5. Example of pushing forces adjustment in the horizontal plane

of the symmetrical voltage applied to the B1–B3 electrode pair in order to orient the pushing force F_{pBc} toward A090°. Depending on the coefficient of friction, the magnitude of F_{pBc} can be increased further by increasing the pressure using stretching (extension) and/or bending of the piezolegs. Similarly, leg C will in most cases be controlled in the same fashion to double the pushing force exerted on the robot to yield a more efficient motion.

Due to the geometry (e.g., diameter of the feet, angle of the piezoleg, etc.), the resulting pushing force will reduce significantly when the leg enters the kinematic state if we assume lower kinetic friction forces as it is typically the case and will be null if the pushing legs are entirely lifted. To create sufficient forces while achieving accurate direction of displacement, we use a simple method that we refer to here as the zero-lag motion, where all bending and stretching forces of all the three legs are synchronized.

3. Fundamental Issues

3.1. Friction

Unlike previous approaches, the performance of the proposed method of motion is extremely sensitive to friction between the feet of the miniature robot and the walking surface. The conventional and simple macro-model of static friction force F_S and a kinetic friction force F_K are stated as

$$F_S = \mu_S F_N; \quad F_K = \mu_K F_N. \tag{5}$$

Here, μ_S and μ_K are the static and kinetic coefficients of friction, respectively, and F_N is the normal force. To achieve the maximum displacement speed, the motion system should operate not only at resonant frequency for maximum amplitudes of deflection of the legs, but the initial force generated by the piezoleg prior to motion must be maximized. In other words, the static coefficient of friction must be set to a specific value such that the resultant static friction force would ideally be slightly inferior to the maximum force that can be generated by each piezoleg.

It can be seen that a change in the mass of the robot will have an impact on the fabrication and the material used for the feet and/or the walking surface in order to tune or adjust the coefficient of friction accordingly. Practically, this is very difficult to achieve due to several constraints that are briefly explained later. Furthermore, the kinetic friction force F_K must be minimized since it generally contributes to decrease the speed of motion of the legs. The relatively small diameter of the spherical feet with an angle of 45° contributes to lower the impact of the kinetic force of friction. At a smaller scale corresponding to the amplitude of the steps, the real models of friction forces are far more complex than the simple model expressed in eq. (5). Among several models, elasto–plastic friction models, for instance, are more accurate, and other factors such as the pre-sliding effects must also be taken into account. It is known that for small displacements such as the deflection amplitude of a single piezoleg for the miniature robot, pre-sliding can be the dominant friction phenomena (Armstrong-Hélouvry, Dupont, and Canudas De Wit 1994). In our particular method of motion, the initial force of the leg to perform each step is created during the stick phase. However, what is classically referred to as static friction is now known to be a regime known as stiction that can extend over several micrometers of motion. Stiction corresponds to the existence of a breakaway displacement, such that for all motion of the friction the interface consists entirely of elastic displacements. Because in solid mechanics the stiction condition is analogous to the existence of an elastic region on a material's stress–strain curve, careful attention must be paid to the choice of materials used for the walking surface and the feet of the robot.

3.2. Material Properties

As mentioned in the previous section, the choice of the materials for the feet of the robots and the walking surface must be selected to provide a stiction force ideally slightly inferior to the maximum force that can be generated by each piezoleg. This will depend on several factors including, but not limited to, the normal force or the mass of each robot and the stress–strain relationship of the materials used for the feet and the

floor. The resonant frequency of one implementation of the piezolocomotion system is ∼ 4 kHz or 4000 steps per second (see Section 5.3) and results in relatively high impacts between the feet and the surface at the end of the phase of each step. Although fast displacements are made with step sizes of the order of a few micrometers, when closer to the target location, step sizes of the order of a few tenths of nanometers are required. In such a case, defects and/or damages caused by such impacts may prevent step size accuracy at the nanometer range. Hence, not only the surface must be polished in a controlled fashion and be extremely flat with minimum defects, but the hardness of the material (presently we use stainless steel 404) used for the feet and the walking surface is also a critical factor. Because the feet of the robot are easier and much less costly to replace after a relatively long wear time, the hardness of the walking surface is selected typically to be slightly higher than the hardness of the feet. Another critical property is the resistance to oxidation and corrosion that would otherwise significantly modify the properties of friction, and hence would affect the performance of the motion system.

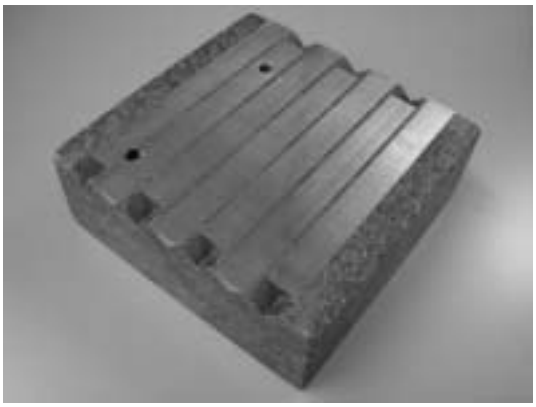

Fig. 6. Small version of the power floor. The holes that appear at the surface are receptacles for special atomic grids designed to position each robot at the atomic scale.

3.3. Power

Because of the too long latency in communication with an external computer, many real-time tasks must be executed by the electronic system embedded onto each robot. The result is that these high-performance miniature robots consume of the order of a minimum of 15–20 W of power on average. In order to maintain the small size of these robots and due to the lack of adequate power sources small enough to deliver the required energy and power density, the power is delivered through the feet of the robots when in contact with the floor. The resulting "power floor" (Martel 2004), as shown in Figure 6, is presently made of electrically conductive bands of stainless steel 440C insulated by a thin non-conductive layer of granite, providing adequate electrical insulation and mechanical/thermal properties. A gap exists between each stainless steel bar and the granite. The width of each gap is maintained to a minimum to allow the robots to transit and to minimize the impact on the motion of the robots, while being large enough to compensate for the thermal expansion of the material within the range of ambient temperatures used in the cooling chamber. The error in motion created through this discontinuity is larger but not critical, since it is corrected prior to the final positioning at a working site.

The width of the bands is selected such that at least one foot of each robot will be in contact with a positive band and at least one foot will be in contact with a negative or ground band, in order to allow electrical current to flow through the embedded electronics of each robot. Hence, in addition to the material properties mentioned in the previous section, the materials must also have good electrical conductivity except for the insulation layer on the power floor. Furthermore, the electrical impedance also related to the contact area between the feet and the floor must be sufficiently low to withstand the relatively high power density. Past experiments have shown that wires make accurate step sizes extremely difficult and affect repeatability. Furthermore, with a potential fleet exceeding 100 miniature robots on a relatively small surface area, the wires would impede the flexibility of displacements throughout the platform.

3.4. Arcing

During motion, the feet may not touch the floor continuously and the small gap between the feet and the floor causes arcing, which due to the relatively high power involved causes substantial erosion that modifies the shapes of the feet and the floor, and hence makes repeatability in accurate motion very difficult. Using an AC instead of a DC voltage level for power would eliminate arcing, but the size of the capacitors embedded onto each robot, and required to regulate the voltage within the requirements of the sensitive embedded electronics, would be too large. In order to reduce the size of the capacitors, a higher modulation frequency could be used; however, considering the amount of power involved, this would increase the risk of excessive coupling noises on the sensitive embedded instruments designed for nanoscale operations. To prevent arcing, a special switching circuit or arcing control circuit is embedded onto each robot. Prior to each step, the onboard processor through the embedded arcing control circuit increases substantially the electrical impedance at the power input prior to each step in order to eliminate or reduce sufficiently the electrical current flowing between the feet and the floor. When in contact with the floor, the arcing control circuit allows a high power density to be delivered to a miniature energy reservoir in the form of a capacitor and

the whole robot then relies on this limited energy source to complete each step. Because of the exponential discharge of the capacitor, increasing the voltage level at the power floor allows more time to execute each step and add flexibility in motion. On the other hand, since the input voltage is regulated to specific voltage levels inside each robot, this flexibility in motion through higher input voltage levels is paid by a reduction of the power conversion efficiency leading to more power dissipated as heat.

3.5. Heat

The Curie temperature where piezoeffects are lost is not the biggest concern here, but rather the limit in temperature that can be applied to the embedded electronics. As the performance of the robots increases with a higher level of miniaturization, the surface available on each robot becomes insufficient to dissipate the heat. In our particular case, this causes an excessive rise in temperature and limits continuous operations for each robot to a few seconds. Using conventional heat dissipation techniques such as heat pipes and/or heat sinks would substantially increase the overall size of the robot. A solution relies on the high heat capacity of water and uses a special multilayer jacket (1 mm thick) installed on each robot. The actual design dissipates heat by evaporating approximately 0.8 g of distilled water. One potential problem is that the total mass of the miniature robot varies by approximately 1.5–2% every few minutes, i.e., between refills. This is another factor that contributes to increase potential errors during motion. To maintain the weight of each robot constant and for continuous operations, i.e., no refills, another approach envisioned is to place all robots in a special cooling chamber. In such a chamber developed especially for cooling a fleet exceeding 100 units and shown in Figure 7, the robots typically operate in a helium atmosphere cooled using liquid nitrogen.

Helium is an inert gas, which is highly suitable for our applications. Furthermore, helium has much higher heat conductivity than air, allowing us to reduce the flow of gas substantially in order to minimize potential thermal drifts on the sensitive instruments and to minimize the impacts on the accuracy of motion of the robots. None the less, the dielectric of helium presents some additional constraints on the design of the piezolegs to avoid arcing.

4. Electronics

Because of the too long latency involved when relying on an external computer, a fair amount of electronics must be embedded onto the robot to provide essential functions needed to operate such a robot in real time. Figure 8 shows the electronic circuit (except for the DC/DC converters and interconnecting wires) implemented with a 12-layer, 500 μm thick, rigid-flex board with components mounted on both side and designed to be bended in a manner depicted in Figure 1.

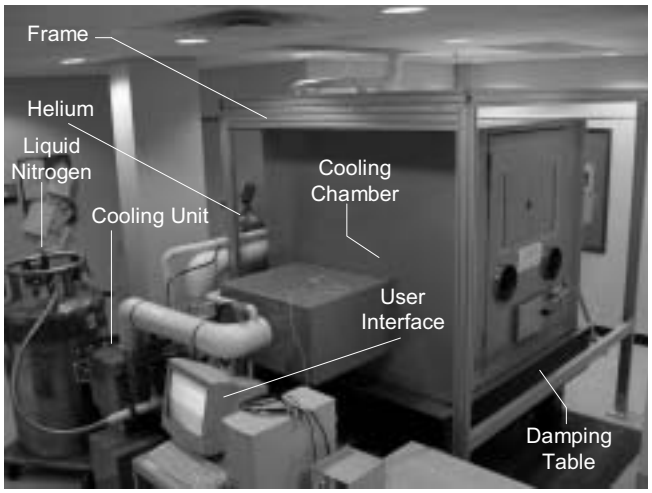

Fig. 7. Photograph of the cooling chamber. This special chamber can support simultaneously a fleet exceeding 100 NanoWalker robots. The interior of the cooling chamber has additional damping systems, wireless communication units, optical positioning units, and various sensors and cables.

The circuit includes an onboard 48 million instructions per second (MIPS) DSP (component 2 in Figure 8) with memory (component 3 in Figure 8), a proprietary controller (component 1 in Figure 8), and a 4 Mb s^{-1} half-duplex infrared (IR) transceiver for communication with an external central computer. The circuit also includes the embedded instrument interface, the power distribution as depicted in Figure 9, which includes the arcing control circuit (shown in the dotted line box in Figure 8) and the switching electronics to drive the three piezolegs (shown in the three thick line boxes in Figure 8) and the drive circuit including the D/A converter for the STM scanner tube, and other miscellaneous functions such as temperature sensors, power amplification, and the bias voltage generation for the STM system, just to name a few.

Typically, piezoactuators are driven using some types of amplitude modulation. This approach generally requires a fair amount of electronics, such as a D/A converter and a power amplifier per quadrant electrode. The quiescent current on each power amplifier increases the continuous load on the $\pm$150 VDC power rails. As a result, the number of DC/DC converters as those depicted in Figure 3 would increase substantially, and hence increases the overall size of each robot.

In order to reduce the size of the robot, the same two DC/DC converters used for the embedded instrument are used for the locomotion system since these two applications do not occur at the same time. To drive the piezolegs, the outputs of the DC/DC converters are frequency-modulated through special embedded switching circuits. Hence, series of high-voltage pulses are used to actuate the legs. Instead of reducing the amplitudes of deflection of the legs by reducing the voltage

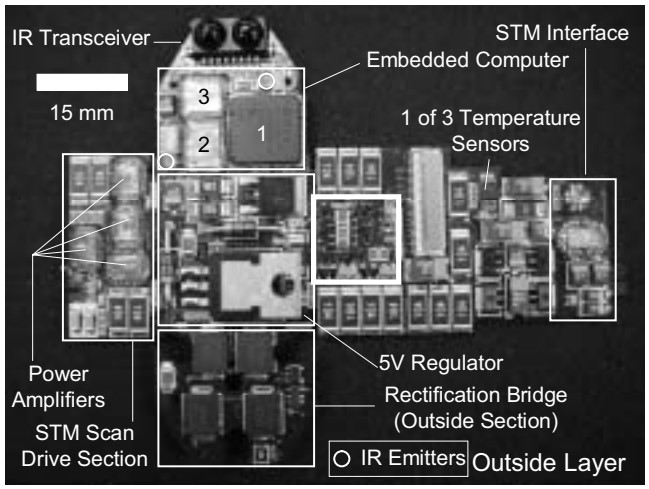

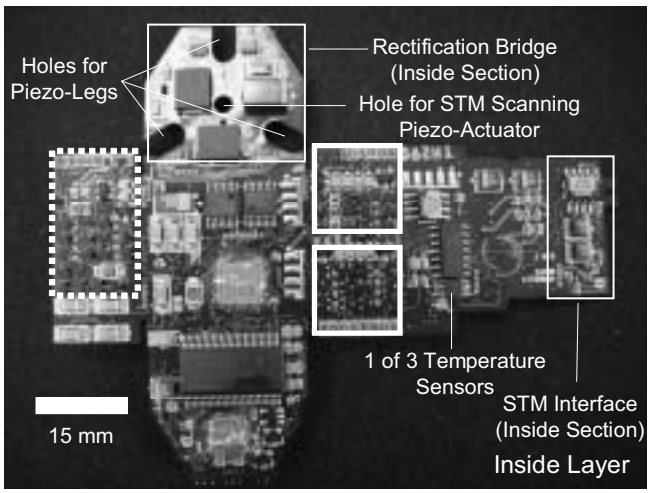

Fig. 8. Photographs of the flexible circuit board for the embedded electronic system.

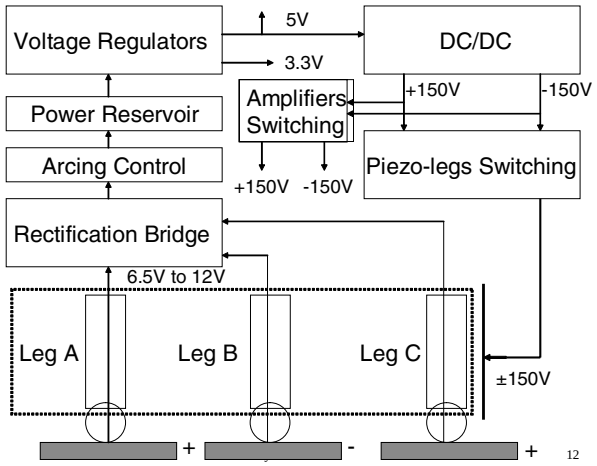

Fig. 9. Simplified diagram of the power distribution system in each robot.

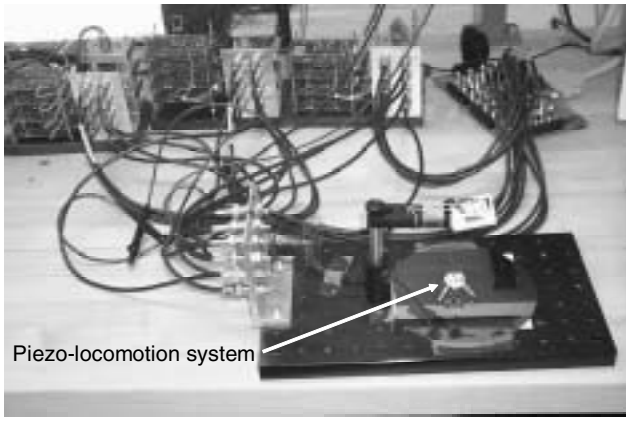

Fig. 10. Photograph of the experimental platform showing the tethered piezolocomotion system on a silicon wafer with the power amplifiers in the background.

amplitudes, the drive signals are generated at a frequency beyond the mechanical resonant frequency of the piezosystem. To create sufficient force for displacement, all three legs are actuated simultaneously. The combination of frequency modulation and phase shifts on each electrodes allows sufficient control for accurate displacements. Although the control of such a scheme is more difficult compared to more traditional methods, the accuracy of the motion system, which is within the deflection range of the embedded scanning tunneling microscope (STM) tip (of the order of ± 70 nm for the present design) is sufficient.

5. Experimental Data

5.1. Experimental Platform

A photograph of the experimental setup used for this study is depicted in Figure 10. A cleaned silicon wafer was used as the walking surface in order to provide a constant static coefficient of friction of 0.25 between the legs of the robot and the walking surface. An underneath plate was used to adjust the wafer in a perfect horizontal plane.

The robot used in this study was tethered with a total of 13 wires: 12 wires were connected to each of the 12 quadrant electrodes and the remaining wire to the ground (the inner electrode of each three legs). The wires connecting to the legs had a very low stiffness and very low weight to minimize variations in motion throughout relatively small distances. Coaxial cables were used between the experimental platform and the power amplification units (see Figure 10). The inputs of the power amplifiers were connected to a custom breakout

board (top right of Figure 10) through coaxial cables. The breakout board was connected to the outputs of a custom-made D/A board providing the 12 18-bit D/A channels with simultaneous updates on all channels.

5.2. Methods

Various walking methodologies have been investigated so far and the proposed push–slip method has proven to be quite effective. The push–slip method presented here uses the phenomenon of stiction as for the stick–slip motion but with different vectored forces. Although many variations of the push–slip motion can be implemented by changing the angles and amplitudes of the resultant forces and/or the synchronization between the legs, the results described in this paper were obtained by using no lag time between the deflections of the legs.

For walking in the A090° direction for instance, the legs A, B, and C were deflected simultaneously toward the A090°, B2B3, and C3C4 regions, respectively, and leg A was considered to be the front leg (leg A is deflecting in the A090° direction or forward in this particular case) while legs B and C were acting as the back legs. In unipolar mode, such a deflection pattern is achieved by applying a positive voltage simultaneously to A1, B2, B3, C3, and C4, but in the symmetric-voltage mode, a negative voltage of the same amplitude is also applied to the counter-electrodes of the back legs B1, B4, C1, and C2. A ratio of –0.85 (i.e., 85% of the reference amplitude) was used instead for the front leg. More specifically, the ratio of voltages referred to the voltage applied to A1 (denoted VA1) applied to the various electrodes was as follows: A1 = 1.0 VA1; A2 = 0.05 VA1; A3 = –0.85 VA1; A4 = 0.05 VA1; B1 = –0.5 VA1; B2 = 1.5 VA1; B3 = 0.5 VA1; B4 = –1.5 VA1; C1 = –0.5 VA1; C2 = –1.5 VA1; C3 = 0.5 VA1; C4 = 1.5 VA1.

Although efficient walking motions have been observed, we do not know at this point if these ratios are optimal under these conditions, and further experimentation will be required. The A1 counter-electrode A3 was set with a ratio of –0.85 instead of –1.0 to compensate for the geometry of the piezotube. The ratio of electrodes A2 and A4 were set to 0.05 instead of 0.0 to cause some small extension in the $-Z$-axis when leg A moves forward. A larger ratio would cause too much extension and increase the pressure between leg A and the walking surface prior to any motion, i.e., when the static force of friction is acting. For the back legs, unlike the front leg, the intended deflections occurred in the pressure zone. For leg B for instance, the deflection force toward B270° (direction of maximum pressure) was 1/3 the deflection force toward B180° (edge of the pressure zone, i.e., minimum pressure). Hence, the resulting deflection force was expected to be toward B210°. With the pressure force combined, the direction of the resulting pushing force was expected to rotate clockwise further. A tangential force acting toward B090° when motion occurs had to be considered as well. This tangential force was the result of the normal force acting on a leg (which typically is 1/3 the total normal force of the robot) and the angle of the leg with the walking surface. When walking in the direction of A090°, B090°, or C090°, the total resultant tangential force is null because of the 60° angle between the longitudinal axis of the two back legs and A270° resulting in a tangential force acting in the opposite direction to the tangential force of the front leg. In such a case, the tangential force of the front leg A adds directly to the force of forward motion where, in the case of the back legs, the B and C tangential forces reduce in the opposite direction the force of pressure exerted to the B3 and C3 quadrants.

The resulting vector for the pushing force on the back legs was therefore dependent upon the resultant force of pressure (the force applied on the B3 or C3 quadrant minus the tangential force of the back legs) and the deflection force exerted on the B2 and C4 quadrants.

The waveform used consists of a periodic triangular shape with the peak at 33% of the period. During the rising edge of the signal, the front leg deflects forward (A090°) while legs B and C exert a pressure on the walking surface while pushing at the same time. This phase causes a momentum forward and, at the same time, the fall period occurs, canceling the deflections on the three legs. Past experiments have shown that using deflection force on the leg in this case really helps to achieve better motion. For instance, the fastest robot motion was achieved when leg A was deflected forward when pushing on the back legs was performed. A pushing action on leg A acting at the same time as pushing on the back legs produces motion at lower speed in the intended direction, and not using leg A at all produces even slower motion in the A090° direction.

5.3. Proof of Concept

A proof of concept has been demonstrated using three four-quadrant 12.5 mm long (PZT-5A) piezoceramic tubular actuators on a prototype that weighed 8 g. Synthetic rubies at the extremities of each leg were used to provide the contact with a silicon wafer. The silicon wafer had a static coefficient of friction of approximately 0.25 (oxidation layer removed) between the legs and the surface. The results showed a maximum displacement speed of 200 mm s^{-1} when actuated at approximately $\pm$40 V and using 4000 steps s^{-1} where step sizes were estimated at approximately 50 μm. Rotation and displacement in a straight line have been achieved as shown in Extensions 1 and 2, respectively. Furthermore, step sizes of approximately 30 nm were achieved; however, due to the stiffness of the wires connecting the piezoactuation system to the electronics, repeatability at such a scale was only feasible on a very short distance and was very difficult to maintain due to the high sensitivity of the system.

As such, to avoid such errors, our design goal was to embed the required electronics to make the robot entirely wireless.

With the electronics depicted in Figure 8, the total mass of the new wireless version is estimated at 32 g. For convenience and to understand the effect of an increase of the mass of each robot, larger values of 88 and 136 g were used in the preliminary experimentation phase.

5.4. Results

The results presented here are based on a prototype of the robot as shown sitting on the wafer in Figure 10. The prototype has been made different from that used for the proof of concept to allow us to increase its mass, which was very difficult to do with the previous prototype (Section 5.3). The second piezoactuation system was built with three legs made from piezoceramic tubes (PZT-5A/EBL #2) of 19 mm in length, 3.175 mm outer diameter with a wall thickness of 0.254 mm. As for the other system, the legs were metallized on the outer and inner surfaces with the outside metal coating sectioned into four quadrants and used as axial segmented exterior electrodes. A 3.175 mm diameter ruby ball terminated each leg.

Figure 11 shows the step sizes that were achieved with various voltages applied to the electrodes using the push–slip method as described earlier. The X-axis lists the bipolar voltages used on electrode A1, with the voltages on other electrodes governed by the aforementioned voltage ratios. For instance, 60 V would mean +30 V on the A1 electrode and 85% (0.85 ratio) of –30 V on the reciprocal electrode A3.

The data obtained suggest that there are threshold voltage levels below which the robot will not move. This threshold effect is due to the fact that the static friction causes a force threshold that needs to be overcome before the robot can move. The data also indicate that these thresholds are dependent not only on the mass of the robot but also on the frequency at which the legs are moving. The graphs of voltage versus step size for push–slip motion also suggest that there is a resonant frequency of approximately 1.31 kHz in this particular experimental version where the fastest motions and the larger step sizes are observed. As shown in Figure 11, increasing the total mass by a factor of 1.54 decreases the maximum step sizes at resonant frequency proportionally, i.e., by a factor of 0.65 in this particular case. For instance, at $\pm$50 V and a total mass of 136 g, the displacement speed at resonance at approximately 1300 steps s^{-1} was measured at 11 mm s^{-1}, which corresponds to a step size of 8.4 μm, showing that there is a somewhat linear correspondence when compared to 12 and 20 μm with 136 and 88 g, respectively. From the results depicted in Figure 11, it is shown that the step size can be changed with a variation of the voltage amplitudes applied (amplitude modulation) and/or the frequency (frequency modulation). It is also shown that depending on the type of surfaces, a minimum frequency is required to achieve motion. In our particular case, a minimum of $\pm$40V was required at 571 Hz (or steps per second) to get any motion. A slight increase in the frequency had a significant impact on the minimum voltage required for motion.

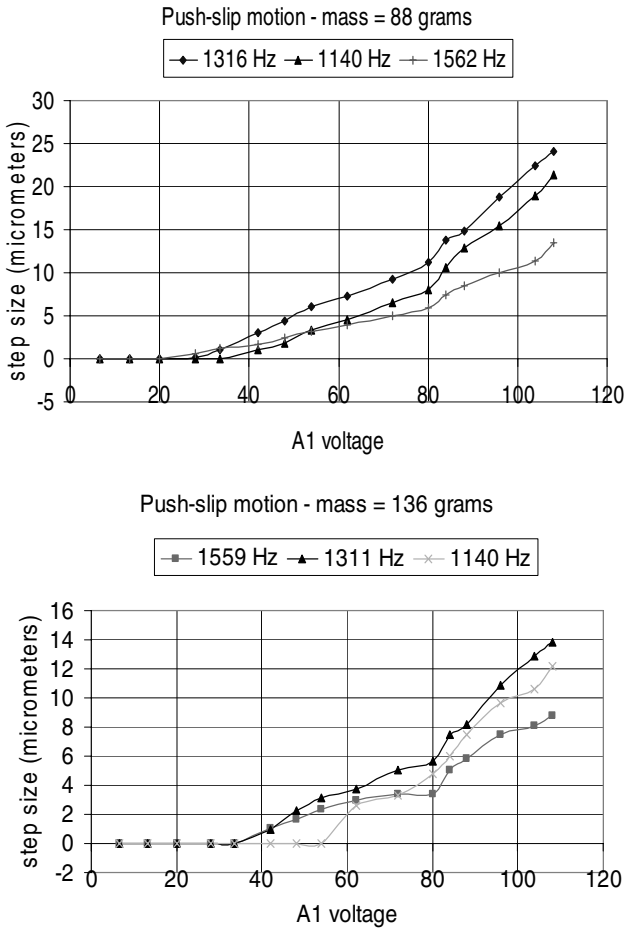

Fig. 11. Step sizes at various voltage levels for the tethered piezolocomotion system with masses of 88 and 136 g.

6. Discussion

The results suggest that a larger voltage produces larger steps sizes at a given resonant frequency. A problem in such a wireless miniature robot is the maximum current available to charge and discharge the capacitance of the electrodes (see eqs. (6a) and (6b) for an estimation of the current requirement in terms of electrical admittance to charge the electrodes assuming that the load is entirely capacitive for simplification) of piezoactuators at a frequency equivalent to the mechanical resonant frequency of the system. This can be problematic from an implementation point of view, especially if the resonant frequency is relatively high.

The mechanical resonance of the floor could also play a significant role during motion, but tuning the frequency using this approach is not an obvious task. The static friction force is expected to play a major role and we believe that fast accelerations can be created by maximum piezoforces (i.e., the maximum static force of friction being slightly inferior to the maximum blocking force of one piezoleg in the bending

mode). As such, the increase of the coefficient of friction in the new power floor (Figure 6) could be exploited to create more force on each leg and potentially decrease the voltage levels applied on the leg to increase the current available to charge and discharge the electrodes at the mechanical or structural resonance. On the other hand, decreasing such voltage would reduce the scanning range of the embedded instrument and this may become a major constraint for positioning and for the tasks to be performed.

Furthermore, it is not entirely clear at this time if we can easily exploit the coefficient of restitution of the floor. For the results provided in this paper, the coefficient of restitution was null whereas for the new power floor (Figure 6) the coefficient of restitution is approximately 0.95.

$$I_{eB} = \frac{V_P}{X_{CB}} = \frac{V_P 0.28\pi^2 K\varepsilon_0\sqrt{D^2+d^2}\sqrt{Y/\rho}}{LN_e \ln(D/d)} \tag{6a}$$

$$I_{eS} = \frac{V_P}{X_{CS}} = \frac{V_P \pi^2 K\varepsilon_0\sqrt{Y/\rho}}{N_e \ln(D/d)}. \tag{6}$$

In eq. (6), the largest voltage swing is $(\pm V_P) < (\pm V_D)$ where V_D is the depolarizing voltage. Y and ρ are the Young's modulus and the density of the material, respectively, and D is the outer diameter of the piezotube. Large Y and small ρ are typically suitable for locomotion. K is the dielectric constant of the piezomaterial, $\varepsilon_0 = 8.85 \times 10^{-12}$ Farad m^{-1}, and N_e is the number of symmetrical outer electrodes of length L per piezoactuator.

7. Summary

We have briefly described the fundamental principles of a locomotion system which is part of the development of a miniature wireless autonomous robot designed to execute sophisticated tasks at the molecular and atomic scales. The robot can perform several thousands of steps per second with step sizes as small as a few tenths of nanometers. The mechanical structure allows an STM tip to be installed. Since the main purpose is to bring an instrument in the form of a miniature robot to the samples, very high precision in movement and positioning is needed in order to move the robot within the limited range of an integrated instrument such as the STM.

The mechanical structure of the robot is built upon a tripod design. The base is made up of three piezoceramic tubes arranged in a conical shape with the apex pointing upward. The end of each tube closest to the surface is capped with a conducting ball for power delivery to the robot. The legs are equidistant to each other, and are at an angle of 45° to the surface. Each tube has four axial segmenting electrodes arranged as four 90° quadrants along the tube or leg. Resting on top of the three legs is a platform on which the electronics and an instrument are attached. Motion of the robot is achieved through bending and stretching of the three legs through applied voltages to the different quadrants of each tube. The friction and the properties of the walking floor are very important parameters.

Since 15–20 W of power is provided to the high-performance embedded electronics of each microrobot through the legs when in contact with the floor, arcing causing fast erosion of the floor and the legs becomes a real concern. A special circuit embedded onto each robot has been developed to compensate for this problem, but this causes constraints on the time available to perform each motion step.

Preliminary results indicate successful motion of the miniature robot using 4000 steps per second with step sizes varying from a few tenths of nanometers to a few micrometers. To achieve a higher level of miniaturization, the typical method of modulation for piezoactuators has been replaced by a series of high-voltage pulses, similar to the method of activation used in insects. It was also found that friction plays a great role and that the properties of the surface of the legs in contact with the floor and the floor itself must be chosen according to several factors. Furthermore, it was found that the effect and the theory of friction at that scale are not very well defined, and this brings uncertainties in the prediction of motion, especially at the nanometer scale.

8. Conclusions

The development of piezoactuation systems for instruments in the form of miniature robots designed for nanoscale operations has many technical challenges. Furthermore, in this paper we have demonstrated that, at such a scale and precision, the development of the locomotion system is highly inter-disciplinary and any decisions in the design phase may affect other components of the system. Hence, in the context of an autonomous system, especially when designed for applications at the nanometer scale, the development of a locomotion system for wireless miniature robots cannot be done independently but by identifying, characterizing, and considering the effects of various parameters not necessarily being part of the robot on the locomotion itself. As the resolution of the locomotion increases, it becomes more sensitive to these parameters, which add substantial constraints on the choice and design of a final autonomous platform, requiring substantial additional research effort.

Appendix: Index to Multimedia Extensions

The multimedia extension page is found at http://www.ijrr.org.

Table of Multimedia Extensions

Extension	Type	Description
1	Video	Rotation using 4000 steps s^{-1} (NanoRotate)
2	Video	Displacement at 200 mm s^{-1} using 4000 steps s^{-1} (NanoFast)

Acknowledgments

This project was previously funded by the Seaver Foundation when the author was at the BioInstrumentation Laboratory at the Massachusetts Institute of Technology (MIT). Presently, the project is supported in part by the Canada Research Chair (CRC) in Conception, Fabrication and Validation of Micro/Nanosystems and grants from the National Sciences and Engineering Research Council of Canada (NSERC), Gouvernement du Québec, and the Canada Foundation for Innovation (CFI). Several students at MIT and EPM also participated in various aspects related to this project.

References

Aoyama, H. and Fuchiwaki, O. 2001. Flexible microprocessing by multiple micro robots in SEM. *Proceedings of the International Conference on Robotics and Automation*, Seoul, Korea, May 21–26, pp. 3429–3434.

Armstrong-Hélouvry, B., Dupont, P., and Canudas De Wit, C. 1994. A survey of models, analysis tools and compensation methods for the control of machines with friction. *Automatica* 30(7):1083–1138.

Breguet, J. M., Pernette, E., and Clavel, R. 1996. Stick and slip actuators and parallel architectures dedicated to microrobotics. *Proceedings of the SPIE* 2906:13–24.

Breguet, J. M., Schmitt, C., and Clavel, R. 2000. Micro/nanofactory: concept and state of the art. *Proceedings of the SPIE: Microrobotics and Microassembly* 4194:1–12.

De Ambroggi, F., Fortuna, L., and Muscato, G. 1997. PLIF: piezo light intelligent flea. New microrobots controlled by self-learning techniques. *Proceedings of the IEEE International Conference on Robotics and Automation*, Albuquerque, NM, pp. 1767–1772.

Drexler, K. E. 1981. Molecular engineering: an approach to the development of general capabilities for molecular manipulation. *Proceedings of the National Academy of Sciences (USA)* 78:5275–5278.

Fahlbusch, S., Fatikow, S., Seyfried, J., and Buerkle, A. 1999. Flexible microrobotic system MINIMAN: Design, actuation principle and control. *Proceedings of the IEEE/ASME International Conference on Advanced Intelligent Mechatronics*, Atlanta, GA, September 19–23, pp. 156–161.

Farrell, H. H. and Levinson, M. 1985. Scanning tunneling microscope as a structure-modifying tool. *Physical Review B* 31:3593–3598.

Ferreira, A., Fontaine, J. G., and Minotti, P. 2000. High precision four-legged walking microrobot using resonant locomotion concept. *Proceedings of the 3rd International Conference on Climbing and Walking Robots (CLAWAR)*, Madrid, Spain, October 2–4.

Fukada, T. and Ueyama, T. 1994. *Cellular Robotics and Microrobotics Systems*, World Scientific, Singapore.

Juhas, L., Vujanic, A., Adamovic, N., Nagy, N., and Borovac, B. 2000. Development of platform for micro-positioning actuated by piezo legs. *Proceedings of the IEEE International Conference on Robotics and Automation*, San Francisco, CA, April 24–28.

Juhas, L., Vujanic, A., Adamovic, N., Nagy, L., and Borovac, B. 2001. A platform for micropositioning based on piezo legs. *Mechatronics* 11(7):869–897.

Martel, S. 2004. Construction of a special surface for power delivery to wireless microelectromechanical systems operating on the same platform. *Proceedings of the 4th International Workshop on Microfactories (IWMF)*, Shanghai, China, Vol. 1, pp. 62–67.

Martel, S. and Hunter I. W. 2002. Nanofactories based on a fleet of scientific instruments configured as miniature autonomous robots. *Proceedings of the 3rd International Workshop on Microfactories*, Minneapolis. MN, September 16–18, pp. 97–100.

Martel, S. and Hunter, I. W. 2004. Nanofactories based on a fleet of scientific instruments configured as miniature autonomous robots. *Journal of Micromechatronics* 2(3–4):201–214.

Martel, S., Madden, P., Sosnowski, L., Hunter I.W., and Lafontaine, S. 1999. NanoWalker: a fully autonomous highly integrated miniature robot for nano-scale measurements. *Proceedings of the European Optical Society (EOS) SPIE Symposium on Envirosens: Microsystems Metrology and Inspection*. Munich, Germany, Vol. 3825.

Martel, S., Bevilacqua, J., Dyer, R., Fofonoff, T., Garcia de Quevedo, W., Helm, C., Sherwood, M., and Hunter, I. W. 2000a. Development of a miniature three-legged bioinstrumented autonomous robot. *Proceedings of the IEEE-EMBS Asia-Pacific Conference on Biomedical Engineering*, Hangzhou, China, September 26–28, pp. 513–514.

Martel, S., Roushdy, O., and Hunter, I. W. 2000b. Miniature instrumented robots for mass-scale synthesis and characterization. *Proceedings of the 1st Annual International IEEE EMBS Special Topic Conference on Microtechnology in Medicine and Biology*, Lyon, France, October 12–14, pp. 160–164.

Martel, S., Saraswat, A., and Hunter, I. W. 2000c. Fundamentals of piezoceramic actuation for micrometer and sub-micrometer motions for the NanoWalker robot. *Proceedings of the SPIE: Microrobotics and Microassembly*, Boston, MA, November 5–6, Vol. 4194, pp. 82–93.

Martel, S., Sherwood, M., Helm, C., Garcia de Quevedo, W., Fofonoff, T., Dyer, R., Bevilacqua, J., Kaufman, J., Roushdy, O., and Hunter I. W. 2001a. Three-legged wireless miniature robots for mass-scale operations at the subatomic scale. *Proceedings of the IEEE International Conference on Robotics and Automation*, Seoul, South Korea, May 21–26.

Martel, S., Riebel, S., Koker, T., Sherwood, M., and Hunter, I. W. 2001b. Large-scale nanorobotic factory automation based on the NanoWalker technology. *Proceedings of the*

8th IEEE International Conference on Emerging Technologies and Automation, Nice, France, October 15–18.

Martel, S., Koker, T., Riebel, S., Sherwood, M., Suurkivi, J., and Hunter, I. W. 2001c. An infrastructure suited for supporting a fleet of wireless miniature robots designed for atomic-scale operations. *Proceedings of the SPIE: Microrobotics and Microassembly*, Newton, MA, October 29–31, Vol. 4568, pp. 221–230.

Martel, S., Cervera Olague, L., Bautista Coves Ferrando, J., Riebel, S., Koker, T., Suurkivi, J., Fofonoff, T., Sherwood, M., Dyer, R., and Hunter, I. W. 2001d. General description of the wireless miniature NanoWalker robot designed for atomic-scale operations. *Proceedings of the SPIE: Microrobotics and Microassembly*, Newton, MA, October 29–31, Vol. 4568, pp. 231–240.

Martel, S., Pelletier, J., Fréchette, A., Azar, A., Valin, B., Poulin, F., Blouin, A., Prud'Homme H., and Hunter I. W. 2002. Toward nanorobotics platforms for high-thoughput biomedical applications at the nanometer-scale. *Proceedings of the 2nd Joint IEEE-EMBS and BMES Conference*, Houston, TX, October 23–26.

Merkle, R. C. 1993. Molecular manufacturing: adding positional control to chemical synthesis. *Chemical Design Automation News* 8:1.

Rembold, U. and Fatikow, S. 1997. Autonomous microrobots. *Journal of Intelligent and Robotic Systems* 19:375–391.

Schmoeckel, F. and Wörn, H. 2001. Remotely controllable mobile microrobots acting as nano positioners and intelligent tweezers in scanning electron microscopes. *Proceedings of the IEEE International Conference on Robotics and Automation*, Seoul, Korea, May 21–26, pp. 3909–3913.

Zollikofer, C. P. E. 1994. Stepping patterns in ants (I. Influence of speed and curvature). *Journal of Experimental Biology* 192:95–106.